Biomedical Investigation of Human Muscle Tissue using Near Infrared Time-Of-Flight spectroscopy

Hampus Mårtensson Jönsson

Bachelor thesis supervised by:
Prof. Stefan Andersson-Engels & Ph.D. Patrik Lundin

Department of Atomic Physics, Lund University

Spring 2015

June 2, 2015

LUND UNIVERSITY
Faculty of Science

Abstract

There are many ways to attain information about human muscle tissue, such as X-ray imaging, tissue sampling, magnetic resonance imaging, e.t.c. One of these methods is photon Time-Of-Flight Spectroscopy (pTOFS). This is a non intrusive spectroscopy method which aids in determining the presence of a substance by means of interpreting its spectral signature and scattering property. The spectral signature is determined by the typical wavelengths that are absorbed by the atoms or molecules.

Photon Time-Of-Flight Spectroscopy utilizes how light propagates through a highly scattering medium, such as tissue, to obtain information about light absorption (spectral signature) and scattering. This is performed by sending many short light pulses into the medium and recording the time it takes for a single photon to reach the detector for each pulse. The scattering and absorption properties of the medium determines the time of flight for a photon before a detection event, which enables a histogram representing the broadening of a light pulse to be built. The absorption and scattering properties of the medium is then extracted by fitting a computer generated theoretical curve or a computer simulated curve to the recorded data.

The study that this bachelor work was based upon refers to measurements on absorption and scattering properties of human muscle tissue for different individuals in the range of 660 to 1340 nm. This to asses if there is any possibility for a trend of these optical properties between different individuals, which could be used for anomaly detection. The results show a promising possibility for this desired trend, but there are uncertainties that make this conclusion difficult to prove. These are for example the small amount of measurements made and the compression of tissue by the used optical fibres.

Abbreviations & Acronyms

AOTF . . . . . Acusto-Optical Tunable Filter
IRF . . . . . Instrument Response Function
MC . . . . . Monte Carlo
NIR . . . . . Near Infrared
PMT . . . . . Photo Multiplier Tube
pTOFS . . . . photon Time-Of-Flight Spectroscopy
RTE . . . . . Radiative Transport Equation
RTT . . . . . Radiative transport theory
SPAD . . . . . Single Photon Avalanche Detector
TCSPC . . . . Time-Correlated Photon Counting
WMC . . . . . White Monte Carlo
μ_a . . . . . Absorption coefficient
μ_s' . . . . . Reduced Scattering coefficient

Contents

[1] Written with Emily Emilsson and can also be found in her bachelor thesis [8].

1 Introduction

A specialisation in the field of applied atomic physics which has gained an increased attention is the field of biomedical optics. In this field properties of biomedical tissue are measured using optical techniques, which have a wide range of different applications. These applications are e.g. diagnosis of lung tumours using both diffuse reflectance and fluorescence spectroscopy [1], photodynamic therapy [2] which treats diseased tissue, and non-invasive gas monitoring in the lungs and intestines of newborn infants using GASMAS (Gas in Scattering Media Absorption Spectroscopy) [3].

Albeit the wide range of techniques that are used in the field of biomedical optics, photon Time-Of-Flight spectroscopy (pTOFS) is a technique which has the advantage of non-intrusiveness, as well as involving minimal patient preparation before measurements. The non-intrusiveness of pTOFS, which means that the tissue under investigation (and its surroundings) is not altered (or needed to be altered), is a property which is desirable for clinical purposes. Photon Time-Of-Flight spectroscopy gives time-resolved measurements which utilizes sub-nanosecond laser pulses, where the pulses propagate through tissue and gain a measurable dispersion. From this time-resolved dispersion the absorption coefficient (μ_a) and the reduced scattering coefficient ($\mu s'$) can be extracted, which reflects the optical properties of the tissue. These coefficients are extracted using a data evaluation method based on White Monte Carlo simulations (see section 2.3).

Even though there already exists a vast amount of research about pTOFS as a tissue diagnosis tool, there has to my knowledge not been any thorough research considering the near infrared optical properties of human muscle tissue for trend-investigation using pTOFS. The aim with this thesis is to investigate the near infrared, NIR1, and NIR2 optical properties of human lower arm muscle tissue using *in vivo* photon Time-Of-Flight spectroscopy, to asses if there is a potential for a trend of these optical properties between different individuals, to enable the detection of anomalies such as tumours. How the amount of subcutaneous arm fat (lipids) and pigment level (included in melanin) affects the absorption and reduced scattering coefficients is also studied.

2 Biomedical Optics

To understand the principles of Photon Time-Of-Flight spectroscopy (pTOFS), which is the measurement technique used throughout this thesis and serves as the main method contributing to the work, one must take the aspects of biomedical optics in mind. Here absorption and scattering of light serves as a basis for the physical phenomena that explain the interaction between light and particles in a medium, which is a basis for the radiative transport theory (RTT), which in turn describes the propagation of light through a medium, such as muscle tissue.

2.1 Optical properties of highly scattering media

A simple way to explain the interplay of light with particles through absorption and scattering is to consider a beam of light incident on a medium. Here some of the light is reflected off the medium, while the rest enters it. The fraction of the light entering the medium mainly interacts with the particles within the medium via absorption or scattering. In what amount the light interacts with the medium, defines the optical properties of the medium. The reason why, is that both absorption and scattering is dependent on the concentration and size of the particles in the medium. The degree of scattering increases with increasing concentration of all particles in the medium, but decreases with increasing particle size, and the degree of absorption increases with increasing concentration of absorbing particles.

Scattering and absorption have two different roles in the interplay between light and particles. Whilst absorption is considered to "eat" all of the photon energy (transferring it to the absorbing particle), scattering has a different role. Scattering occurs in two ways, inelastic or elastic. The contribution of inelastic scattering is ignored in this thesis because of the low probability of occurrence in comparison with elastic scattering. Elastic scattering such as Mie scattering and Rayleigh scattering, has the property of preserving the energy of the photon whilst changing its direction. Mie scattering occur when the wavelength of the light is comparable with the particle size (or is smaller), and Rayleigh scattering occur for wavelengths larger than the particle size. Rayleigh scattering has a $1/\lambda^4$ wavelength dependence and Mie scattering has a $1/\lambda^b$ dependence, where $b < 4$ is a constant.

The amount of absorption and scattering in the medium is defined by the absorption coefficient μ_a [cm^{-1}] and the scattering coefficient μ_s [cm^{-1}] respectively. μ_a describes the absorption probability per unit length in the medium and μ_s describes the respective for scattering. Another parameter which is needed to take into consideration for highly scattering media (turbid media), e.g. human tissue, is the reduced scattering coefficient, μ_s', given by (1) [4]

$$\mu_s' = (1 - g)\mu_s \tag{1}$$

Here $g = < cos\theta >$ is the anisotropy factor describing angular distribution of

scattered light in the medium, g represents the tendency towards forward scattering and undertakes values between 0 and 1. As g approaches 1 the light in the medium is considered heavily forward scattered [5].

How much the light penetrates the medium before getting absorbed is described by the mean free path before absorption and is given by $1/\mu_a$. The path length before scattering is correspondingly described by the mean free path before scattering, i.e. $1/\mu_s'$.

2.2 Radiative transport theory[1]

The Radiative Transport Theory (RTT) does not utilize the wave equation, instead it deals with the energy transport of particles through a medium of random particles [6]. In this theory light is portrayed as independent moving particles that do not interact with each other, which expresses the energy balance within a certain volume in consistence with energy conversation. However, the light particles, i.e. photons do interact with the particles within the medium by means of scattering and absorption. Energy transfer coupled to absorption is considered to be heat and the scattering is considered to be elastic, i.e. that the direction of propagation is changed, but the energy is conserved.

The RTT can be expressed by an equation called the Radiative Transport Equation (RTE) (8). The way to do this is to first consider a small volume, V, with a surface area, A, a specific direction, $\hat{s}$, and the possible events that can occur in the volume. The possible events are [7]:

- Radiation through the surface boundaries.
- Scattering into a direction different from $\hat{s}$ or the absorption of a photon in the medium.
- Scattering from directions $\hat{s}'$ into the $\hat{s}$ direction.
- Radiation from a source inside the medium.

These different events are described by equations (3), (4), (5), (6) and (7) [4].

Equation (2) describes how the number of photons in the volume V and the direction $\hat{s}$ changes with time t in position $\bar{r}$.

$$\int_V \frac{\partial N(\bar{r},\hat{s},t)}{\partial t}\, dV = \int_V \frac{\partial N}{\partial t}\, dV \equiv \left(\frac{\partial N}{\partial t}\right)^V \tag{2}$$

Radiation through the surface boundaries either cause a loss or gain of photons depending on if they are exiting or entering the volume respectively. How the

[1] Written with Emily Emilsson and can also be found in her bachelor thesis [8].

number of photons N change with time t in the volume regarding the surface boundaries with area A is described by equation (3). In this equation c is the speed of light in the medium and $\hat{n}$ is the refractive index.

$$\left(\frac{\partial N}{\partial t}\right)^{V}_{transfer} = -\int_{A} cN\hat{s}\cdot\hat{n}\ dA = -\int_{V} c\nabla N\cdot\hat{s}\ dV \tag{3}$$

Equation (4) describes how the number of photons in the volume change with time due to absorption, and it is dependent on both the speed of light in the medium c and the absorption coefficient μ_a.

$$\left(\frac{\partial N}{\partial t}\right)^{V}_{a} = -\int_{V} c\mu_a(\bar{r})N\ dV \tag{4}$$

The changes due to scattering in directions $\hat{s}'$ from $\hat{s}$ can be described by equation (5) which is the same as the equation handling the changes due to absorption with the only difference being the dependence of the scattering coefficient μ_s instead of the absorption coefficient μ_a.

$$\left(\frac{\partial N}{\partial t}\right)^{V}_{s_-} = -\int_{V} c\mu_s(\bar{r})N\ dV \tag{5}$$

Equation (6) describes the changes in the number of photons due to scattering events that causes photons to change from a direction $\hat{s}'$ into the direction of interest $\hat{s}$. The equation depends on the scattering coefficient μ_s, the speed of light in the medium c and a probability function $p(\hat{s}', \hat{s})$.

$$\left(\frac{\partial N}{\partial t}\right)^{V}_{s_+} = -\int_{V} c\mu_s(\bar{r})\left(\int_{4\pi} p(\hat{s}', \hat{s})N(\hat{s}')\ d\omega'\right)\ dV \tag{6}$$

Sources inside the medium are taken into account using a source function $q(\bar{r}, \hat{s}, t)$ which is describing the gain of photons due to the source in the medium. Equation (7) describes this gain of photons in the medium.

$$\left(\frac{\partial N}{\partial t}\right)^{V}_{source} = \int_{V} q(\bar{r}, \hat{s}, t)\ dV \tag{7}$$

When combining equations (3)-(7) and considering that the volume is arbitrary one obtains the RTE (8).

$$\frac{\partial N}{\partial t} = -c\nabla N\cdot\hat{s} - c(\mu_a + \mu_s)N + c\mu_s\int_{4\pi} p(\hat{s}', \hat{s})N(\hat{s}')\ d\omega' + q \tag{8}$$

2.3 Monte Carlo [1]

A way to solve the RTT is by using Monte Carlo (MC) modelling, which is a statistical modelling method. The principle of this model is to trace the trajectory and interactions (events) of a packet of particles (which could be thought of as photons) in a turbid medium by simulating a number of random walks. After each event the number of photons in the photon packet (weight) has a probability of being reduced by absorption. The remaining photons continue in a random direction until a new event occurs. For every event a probability function is needed for a number of variables, such as:

- The scattering probability governed by μ_s'.
- The absorption probability governed by μ_a
- The step length, i.e. how far the photon propagates before being either scattered or absorbed.
- The direction of the photon after each event.

The mentioned step length before each event can be generalized by the following equation (e.q (5.7) [5]):

$$s_1 = \frac{-ln(RND_1)}{\mu_t} \tag{9}$$

where s_1 defines the step length, RND_1 is a random number between $[0, 1]$, and $\mu_t = \mu_a + \mu_s$. The photon packet is considered terminated when the photons either get absorbed or leaves the area of interest (medium).

In this bachelor thesis a version of the MC model called White Monte Carlo (WMC) is used. The main difference is that in WMC the absorption is added at the end of the solution. For more information regarding the MC and the WMC models see [5,7,9].

2.4 Photon Time of flight spectroscopy

The photon time of flight spectroscopy technique is a method made to obtain μ_a and μ_s' separately. This task is not possible for ordinary absorption spectroscopy, which only depend on intensity. The importance of intensity for pTOFS is to obtain a good signal to noise ratio, but the phenomenon making pTOFS possible is that the path of different photons propagating through a scattering medium is somewhat random. This leads to different path lengths and thus different time-of-flights for the photons. The utilization of pTOFs to determine μ_a and μ_s' thus depend on how a short laser pulse is broadened in time after passing through a medium. An illustration of the mentioned pulse broadening can be seen in figure 1.

[1] Written with Emily Emilsson and can also be found in her bachelor thesis [8].

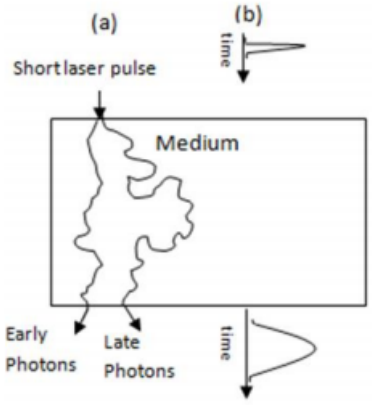

Figure 1: An illustration of how photons from a short laser pulse are scattered while propagating through a medium (a), and how the laser pulse is broadened in time (b) [10].

The change in the laser pulse profile as a response of changing the absorption and scattering coefficients is illustrated in figure 2.

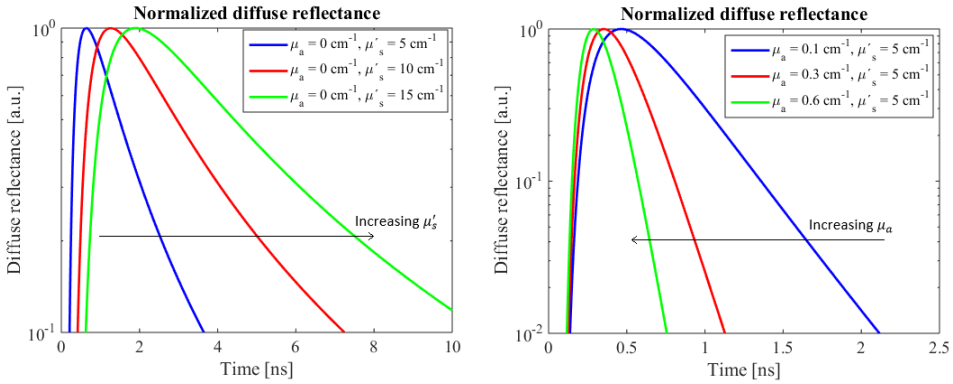

Figure 2: An illustration of how a laser pulse is broadened in time by changing either μ_a or μ_s'.

The pulse profile broadens by increased scattering due to the mean free path before scattering being decreased, which leads to a higher number of scattering events for photons travelling a certain distance, and thus increasing the time of flight. The effect of increased absorption is on the contrary a narrowing of the time of flight pulse profile, where photons that are taking longer paths undergoes a greater dampening.

For each measurement made, an Instrument Response Function (IRF) is generated. The IRF has the function of giving feedback on the system response for light not going through the sample, and thus aids in evaluating the measurements with higher accuracy. A very precise system is needed to differentiate the path length of individual photons in time resolution. The system used in this thesis, like any real system, does contribute to a temporal drift over time. This temporal drift is compensated for by splitting off a small part of the laser pulse and sending it directly to the detector (a time reference pulse). As a result, the

IRF and the experimental data can be matched in time by observing the possible shift of the time reference signal, to compensate for any temporal drift. Figure 3 shows an example of a time reference pulse and a IRF.

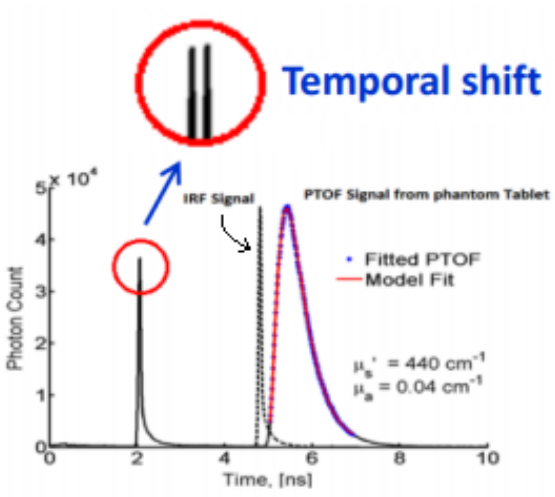

Figure 3: An illustration of a model fit showing the IRF, measured data, and the time reference. The time reference pulse is represented by the sharp peak at 2 ns. *Modified from [11].*

2.5 Human tissue

2.5.1 Optical properties of biological tissue

The microscopic variations of the refractive index existing in tissue (averaging around 1.4) are responsible for the massive scattering biological tissue exhibits. Tissue has high scattering and absorption in the Ultra-violet spectral region, which yields short optical penetration depths and thus poor applicability for tissue spectroscopy. The visible and near-infrared spectral regions (400 to 1350 nm) corresponds to weaker absorption (light is thus regarded as diffuse after travelling a shorter distance) followed by a longer penetration depth, which gives higher usability for biomedical optics.

There is a particular wavelength region of interest in biomedical optics, named the *tissue optical window*. This "window" spans from approximately 600 to 1000 nm and the absorption here arises primarily from haemoglobin (oxygenated and deoxygenated), melanin (pigments) and water [4]. An illustration of the tissue optical window is shown in figure 4.

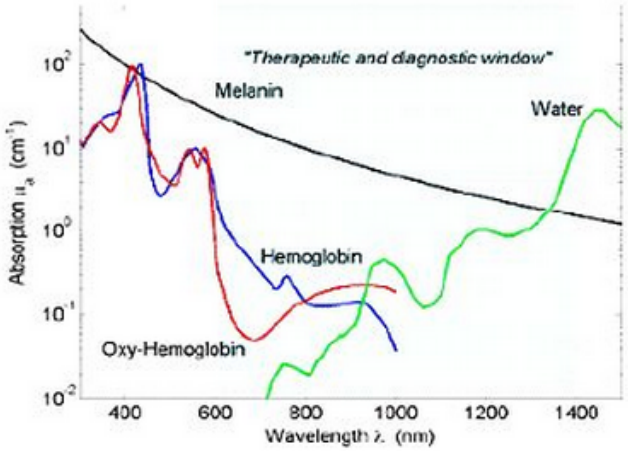

Figure 4: The tissue optical window [12].

Above 900 nm the chromophores that give considerable affect to absorption are mainly water, melanin, collagen, elastin, and lipids (see figures 4 and 5). Lipids which e.g. are present in the subdermis, have a prominent absorption peak at 1210 nm. The main factor limiting the extension of the tissue optical window to longer wavelengths is the absorption due to water.

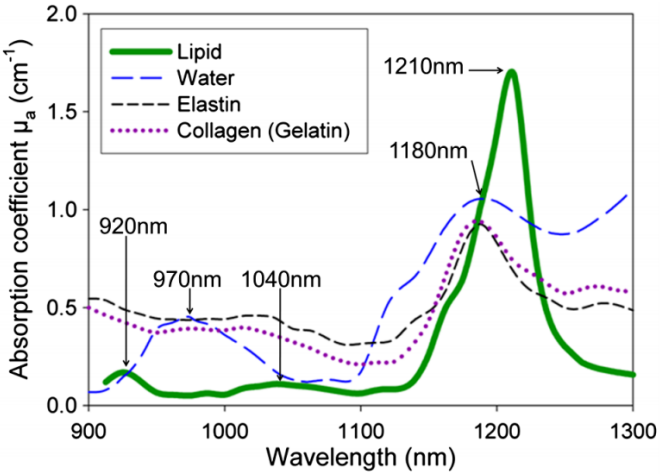

Figure 5: Absorption coefficient spectra for lipid, water, elastin, and collagen above 900 nm *[13].*

2.5.2 Muscle tissue

The composition of muscle tissue is based on bundles of individual components of muscle fibres held together by connective tissue, which simultaneously works as a pathway for nerves and blood flow into the muscle. Mentioned muscle fibres are made from myofibrils, which are long cylinders of about 1-2 μm in diameter. The main absorption characteristics of muscle tissue is given by water and haemoglobin [14].

3 Instruments and method

3.1 Set up & Components

An illustration of the experimental set up with its components used in this thesis is shown in figure 6.

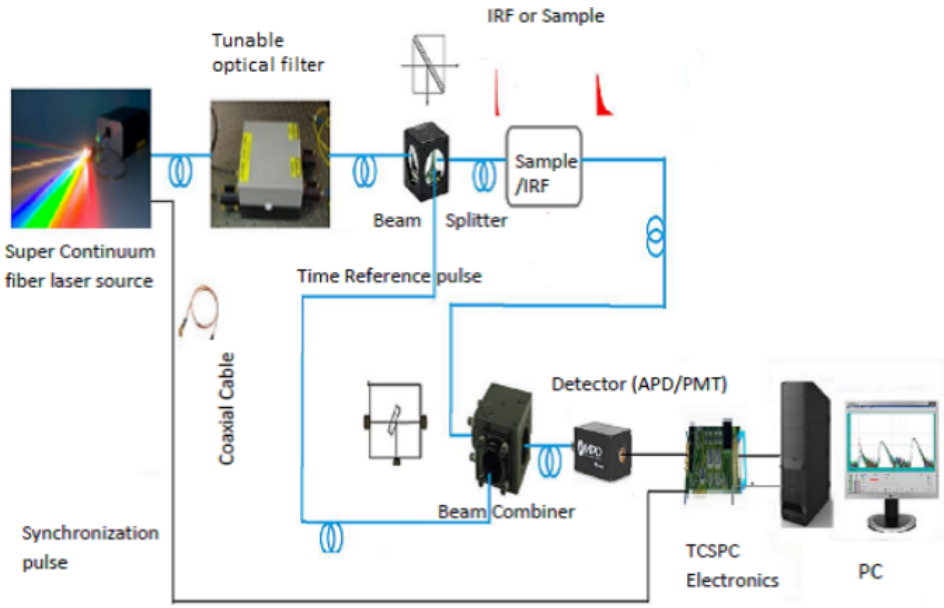

Figure 6: An illustration of the experimental set up used in this thesis. Modified from [10].

3.1.1 The light source, a super-continuum laser

A Fianium SC-480-10 laser which provides a total power of $10\ \mathrm{W}$ were used. This laser operates in the $80\ \mathrm{MHz}$ repetition range with a fundamental pulse width of 6 nm, and has a light output between 480 and 2400 nm. The SC-480-10 laser consists of a core pumped Yb-doped fibre laser (passively mode locked) coupled to a laser diode pumped amplifier and a highly non-linear optical fibre which generates the broad spectrum [15].

3.1.2 Filters

Two different optically tunable filters provided by Fianium were used. The first filter used is an Acusto-optical Tunable Filter (AOTF), which can vary the output wavelength dependent on an acoustic wave generated from an Acusto-optical modulator unit. The AOTF filter consists of birefringent crystals which have the refractive index depending on an acoustic wave which generates acoustic pressure. The result is a created grating in the crystal which scatters incoming light dependent on wavelength. The AOTF used in this thesis is a AOTF-Dual system having two crystals. One of the crystals has output for near infrared (NIR) light

spanning from 650 to 1000 nm (NIR1), and the other crystal has output for visible light spanning from 400 to 690 nm.

The second filter used is a Laser Line Tunable Filter (LLTF), named Fianium LLTF Constrast SWIR which can be tuned for output between 950 and 2300 nm. It is based on Bragg Tunable Filter technology and utilizes a periodically varying refractive index. This enables constructive interference for a certain narrow wavelength band dependent on the angle of the incoming light [15].

3.1.3 Attenuators

The attenuators used in this thesis were made by OZ Optics LT. The ones used for the SPAD detector (see 3.1.4) have a tunable attenuation between -40 and -2.6 dB and the ones used for the PMT detector (see 3.1.5) have a tunable attenuation between -30 and -2.6 dB. These attenuators are needed to protect the detectors from being exposed by light of too high intensity, and to make sure that the rate of photons is low.

3.1.4 Detectors

Two different kinds of single photon counting detectors were used in this thesis. These detectors cover different wavelength regions.

3.1.4.1 SPAD detector

The detector used for wavelengths under 1000 nm is a Single-Photon Avalanche Photo Diode (SPAD) detector named PDM100ct, provided by Micro Photon Devices. It has a wavelength detection region spanning from 375 nm to 1000 nm. The detector has a photon detection efficiency of 49% at 550 nm and generates a TTL output pulse per detected photon [16].

3.1.4.2 PMT detector

A Micro-Channel Plate Multiplier Tube (MCP-PMT) with a InP/InGasP photo cathode was used for wavelengths above 1000 nm. The used detector (R3809U-68), provided by Hamamatsu Photonics has a wavelength detection region from 950-1400 nm. This detector needs to be cooled down to about $80^{\circ}\mathrm{C}$ to reduce thermal noise and to enhance sensitivity.

3.1.5 TCSPC

The used Time-Correlated Single Photon Counting (TCSPC) module in this thesis is a SPC-130-EM provided by Becker & Hickl GMBH. TCSPC is considered to be a very efficient technique for highly time resolved single-photon detection and the principle of the technique is to measure the time delay between two events, such

as between a photon arriving at a detector and a reference signal. A statistical distribution of the time delay can be obtained by repeating the same measurement several times.

The used module operates in the start-stop mode, which implies the importance of starting the clock when a photon is detected and stopping the clock when the next reference pulse (from the laser) arrives at the detector. The importance of using the reversed start-mode arises from the TCSPC module needing a reset time, which otherwise would prevent early photons from being detected.

3.2 Software

In this bachelor work, Computer software is accountable for the control of the hardware as well as data evaluation.

3.2.1 LUNDtofs

The LUNDtofs program made by the Lund biophotonics group, controls the filters and the attenuators. It also displays and stores the output from the TCSPC card showing a histogram and a numerical value of counts per second. The program allows the user to set a desired wavelength range to measure, and it has variable settings for desired count rate. Each wavelength is collected 25 times for better accuracy. The count rate can be increased by changing the collect time and the attenuation level. Before performing actual measurements, calibration of the attenuation level is required, which allows the program to know the relation between count rate and attenuation, which in turn allows the program to adjust the time reference peak during measurements.

3.2.2 Timeresolved v3

Evaluation of the measured data is made by the matlab based program Timeresolved. It is created for the Lund Biophotonics group and is a curve fitting tool utilizing both the Monte Carlo and the diffusion model. The program allows the user to import desired spectral files to which it locates the peaks and removes incorrect peaks (outliers). A sum is made for all the 25 sets for each wavelength to which the program tries to perform the best fit using the user chosen model (per say. White Monte Carlo).

3.3 Performing the measurements

Two different systems using the components described in section 3.1 are used, i.e. one for the SPAD detector and one for the PMT detector. The principle of the measurement procedure is very similar for both systems and can be described jointly. An example of how a measurement is performed on a patient is shown in figure 7.

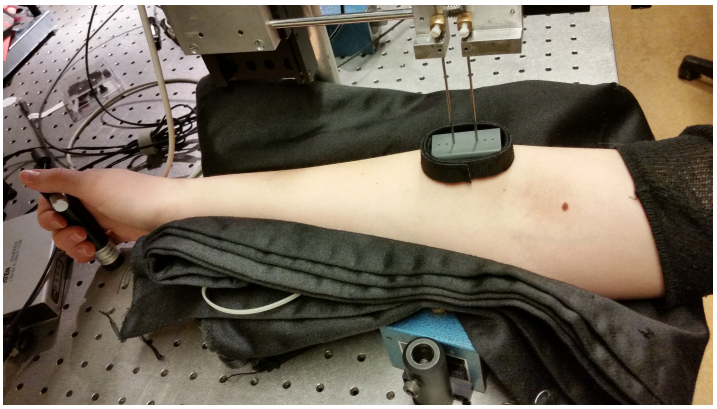

Figure 7: An example of the patient set up used for the measurements.

The measurements are performed by having two fibres in contact with the skin of a lower arm of a patient. These fibres correspond to the source fibre (arising from the light source) and the sample fibre (going to the detector from the patient) respectively. The fibres are not pressed down into the skin to preserve the semi-infinite geometry desired. A small block is put in between the fibres to prevent leakage between them and thus assuring that the measured signal arises from light having passed through tissue. The arm is fixed in a permanent position during the measurements to preserve physical properties such as geometry and net blood flow. This patient set up is used for both detector systems.

The wavelength range measured using the SPAD detector and the PMT detector is 660-1000 nm (NIR1) and 950-1340 nm (NIR2), respectively. The hardware for the measurements is controlled by the LUNDtofs program and the evaluation of the measured data is made by "Timeresolved v3" using the White Monte Carlo template for semi-infinite tissue. The measurement procedure described is made on four different patients.

4 Results

The first set of measurements were conducted in the range of 660 to $1000\ \mathrm{nm}$ in step of $10\ \mathrm{nm}$, using the AOTF in the NIR1 Range and the SPAD detector. The fibre separation was set to $15\ \mathrm{mm}$. Eight measurements in total on four different subjects were conducted using the SPAD detector. Three measurements were conducted on a female subject (pale coloured skin), three on one of the male subjects (male 1, light brown skin tone), and the two other subjects (male 2, paled coloured skin, and male 3, more muscular with a darker skin tone) were measured on only once. Note that the measurements were made on different days. The results from these measurements are presented in figures 8-11. For matters of consistency and for comparison, the subjects who have undergone several measurements have their mean spectrum plotted in figures 10 and 11.

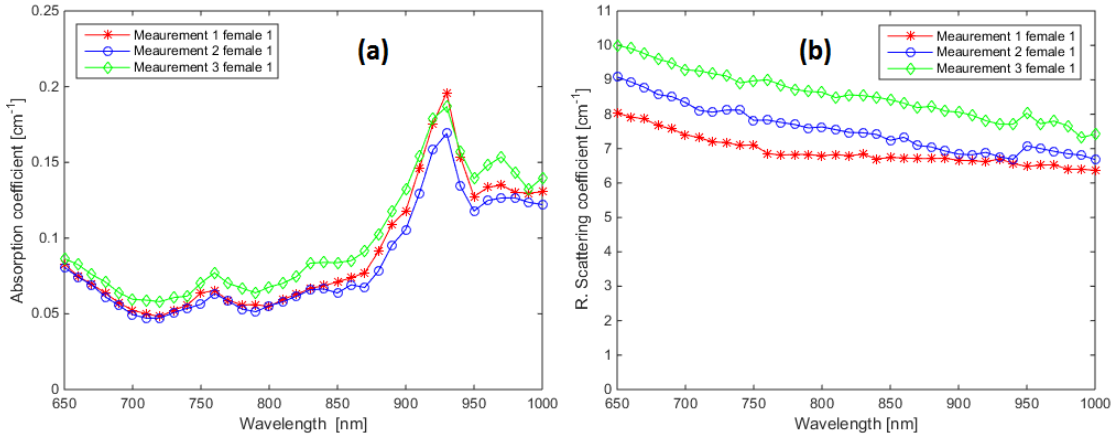

Figure 8: Measured absorption (a) and scattering (b) spectra for muscle tissue with 15 mm *fibre separation. The legends shows the chronological order of the measurements made on the female subject.*

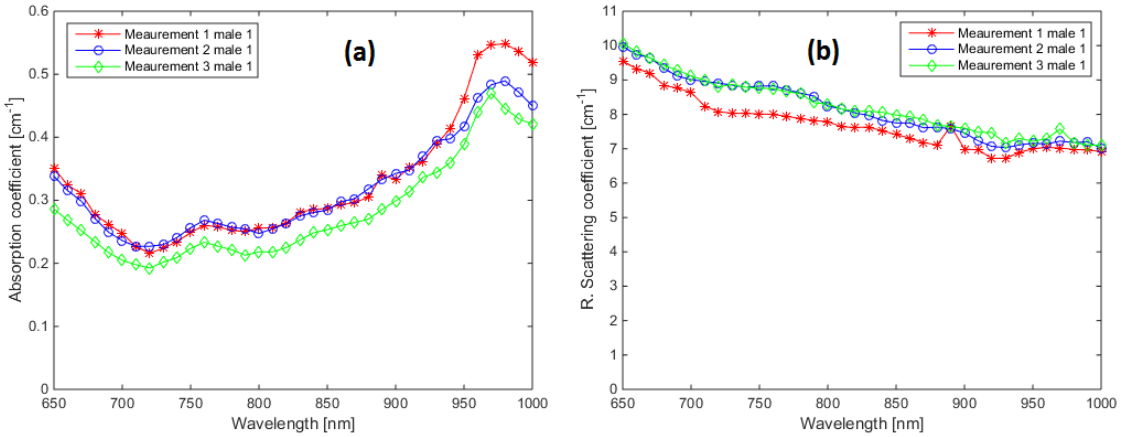

Figure 9: Measured absorption (a) and scattering (b) spectra for muscle tissue with 15 mm *fibre separation. The legends shows the chronological order of the measurements made on the male subject.*

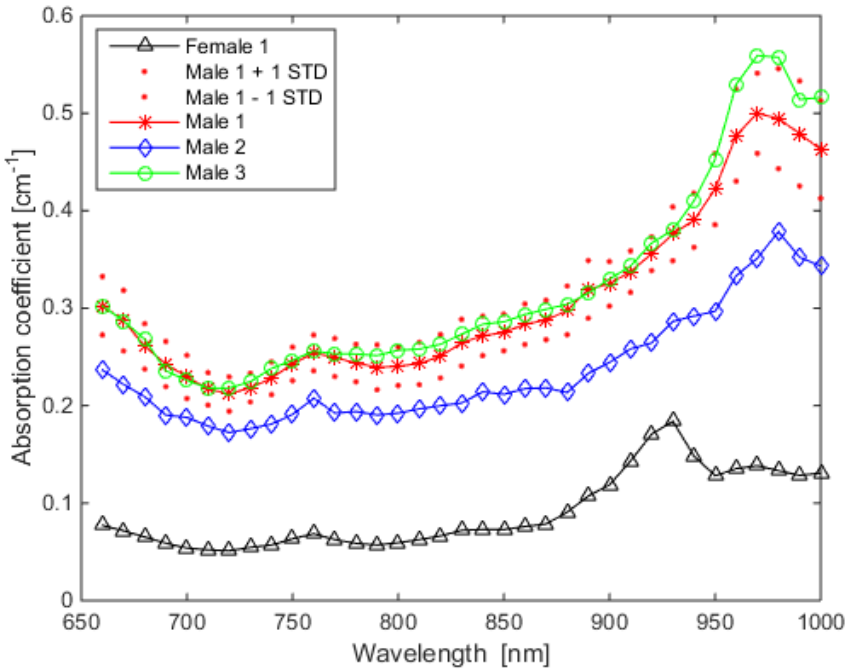

Figure 10: Measured absorption spectra for muscle tissue with 15 mm *fibre separation. The legend displays which data corresponds to which test subject. The standard deviation (STD, dots) for the three measurements made on male 1 is also also presented.*

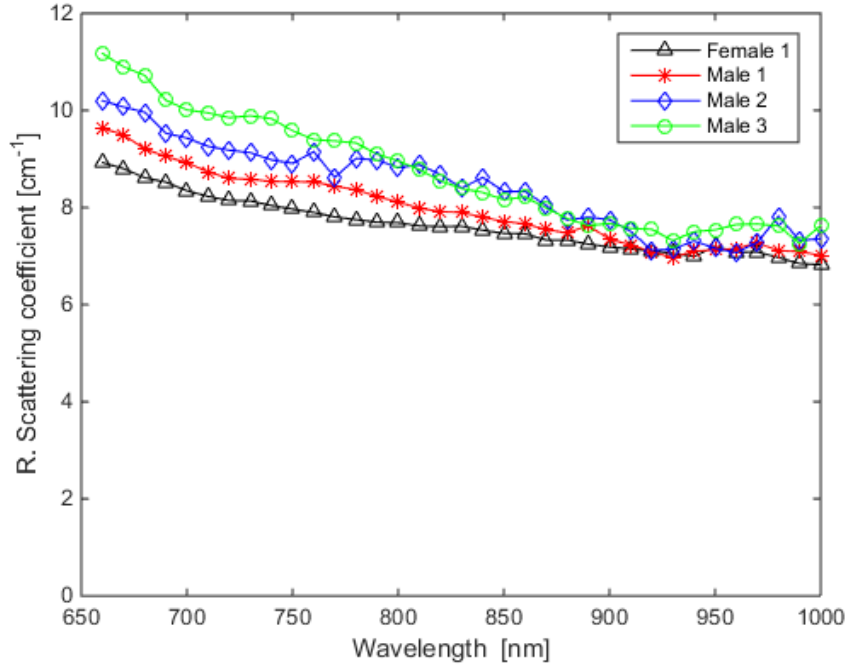

Figure 11: Measured scattering spectra for muscle tissue with 15 mm *fibre separation. The legend displays which data corresponds to which test subject.*

The spectra obtained by the measurements represented in figure 10 were interpolated with reference data on μ_a for water, HbO_2, HB, melanin, and lipid from [18], to obtain a spectral fit which can e.g. extract the relative melanin concentration and lipid concentration of the different subjects. The resulting fit for each test subject is shown in figure 12 and the corresponding melanin concentration and lipid concentration is shown in table 1.

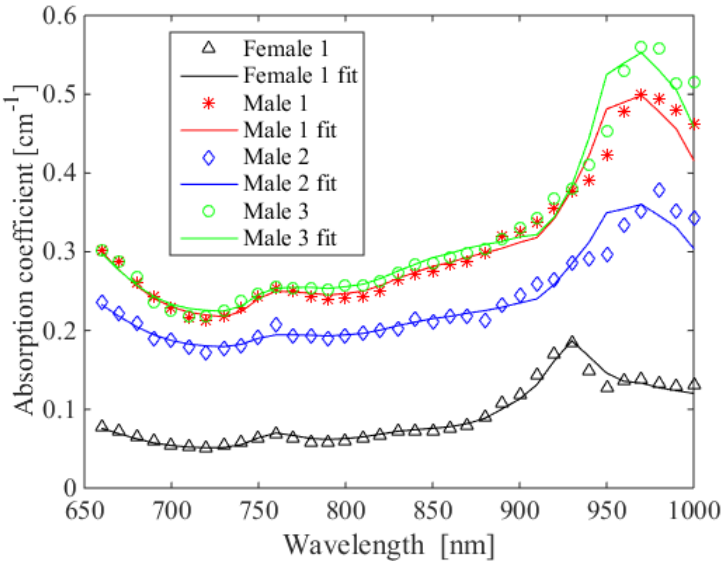

Figure 12: The acquired spectral fit to the measured data represented in figure 10 obtained by reference data on the μ_a for water, HbO_2, HB, melanin, and lipid.

Table 1: The relative melanin concentration and lipid concentration for the test subjects obtained by the fit represented in figure 12. The negative value of the lipid concentration for Male 3 is discussed in section 5.2.

Test Subject	Melanin concentration [a.u.]	Lipid concentration [a.u.]
Female 1	0.082	7.060
Male 1	0.632	1.097
Male 2	0.636	1.400
Male 3	0.685	-0.438

The second set of measurements were conducted in the range of 950 to 1340 nm in step of 10 nm, using the LLTF in NIR2 Range and the PMT detector. The fibre separation was set to 15 mm. Here, six measurements were made in total on four different subjects. Two measurements were made on a female subject and two were made on one of the males (male 1). See figures 13-16 for the results. The measurements were not conducted on the same day, and the subjects who have undergone several measurements have their mean data plotted in figures 15 and 16.

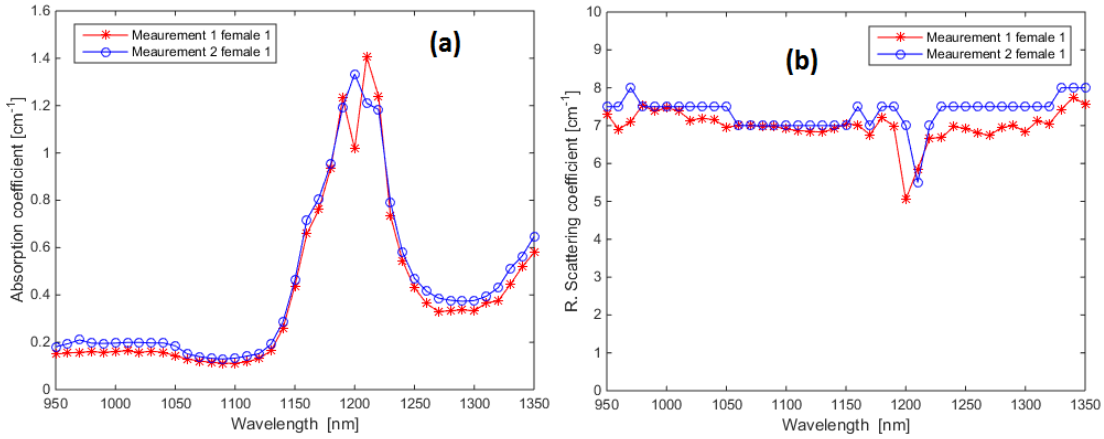

Figure 13: Measured absorption (a) and scattering (b) spectra for muscle tissue with 15 mm *fibre separation. The legends shows the chronological order of the measurements made on the female subject.*

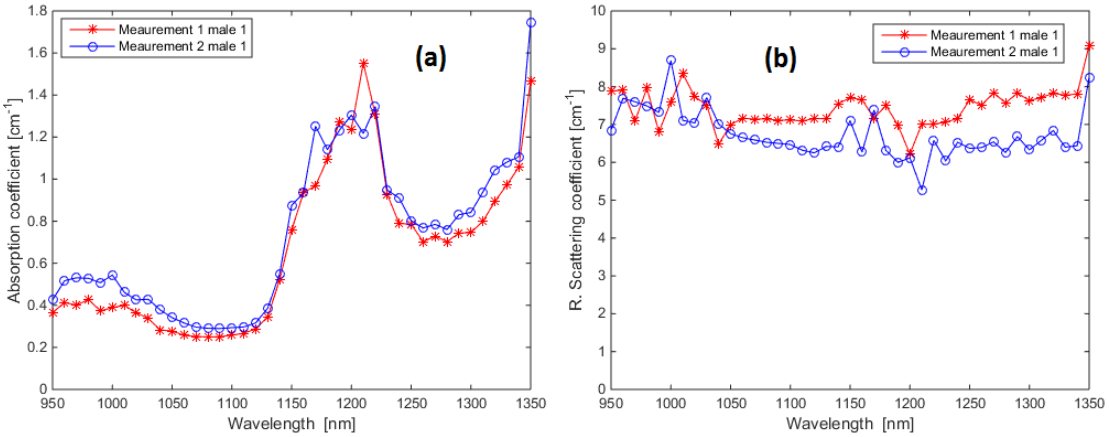

Figure 14: Measured absorption (a) and scattering (b) spectra for muscle tissue with 15 mm *fibre separation. The legends shows the chronological order of the measurements made on the male subject.*

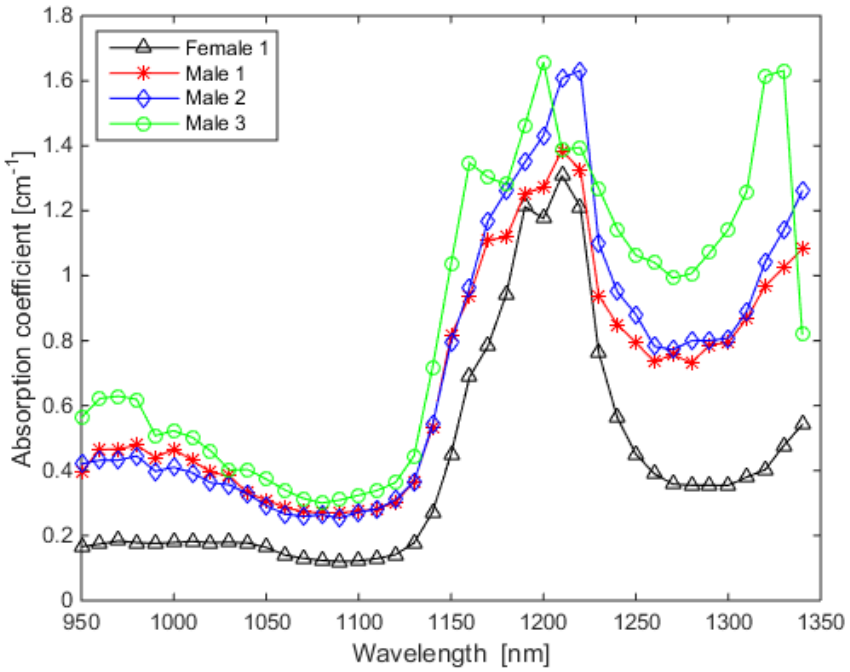

Figure 15: Measured Absorption spectra for muscle tissue with 15 mm *fibre separation. The legend displays which data corresponds to which test subject.*

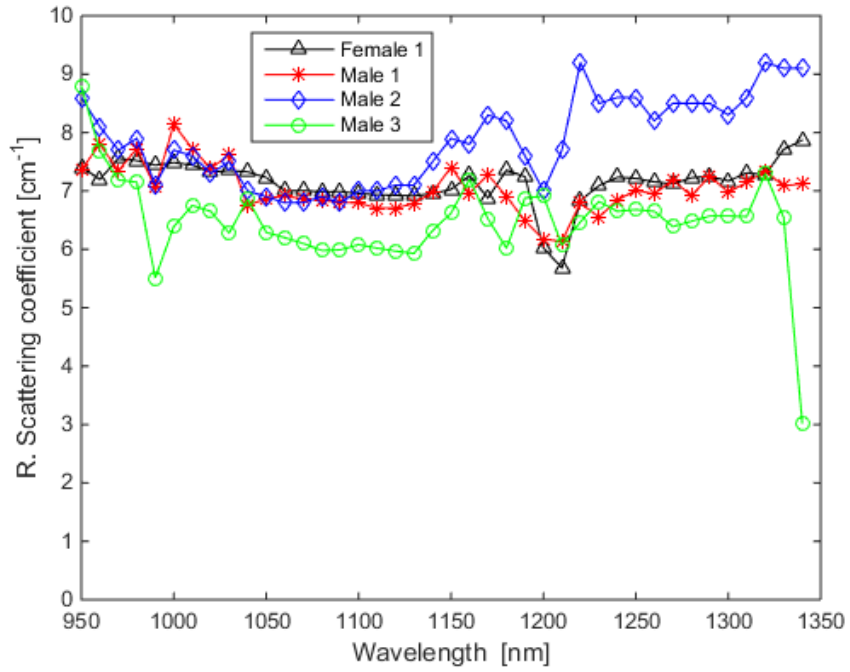

Figure 16: Measured scattering spectra for muscle tissue with 15 mm *fibre separation. The legend displays which data corresponds to which test subject.*

5 Discussion & Analysis

5.1 Validating the measurements

5.1.1 The SPAD detector system

Validating the measured data shown in figures 8-16 is important to verify the relevance of the measurements, and thus important for the purpose of this thesis. There are studies conducted on the absorption and scattering spectra for human tissue, and in this thesis, the measured data is compared to the data obtained by [7] and [19]. Figure 17 shows data taken by [7] and [19] for the NIR1 range using 20 mm fibre separation.

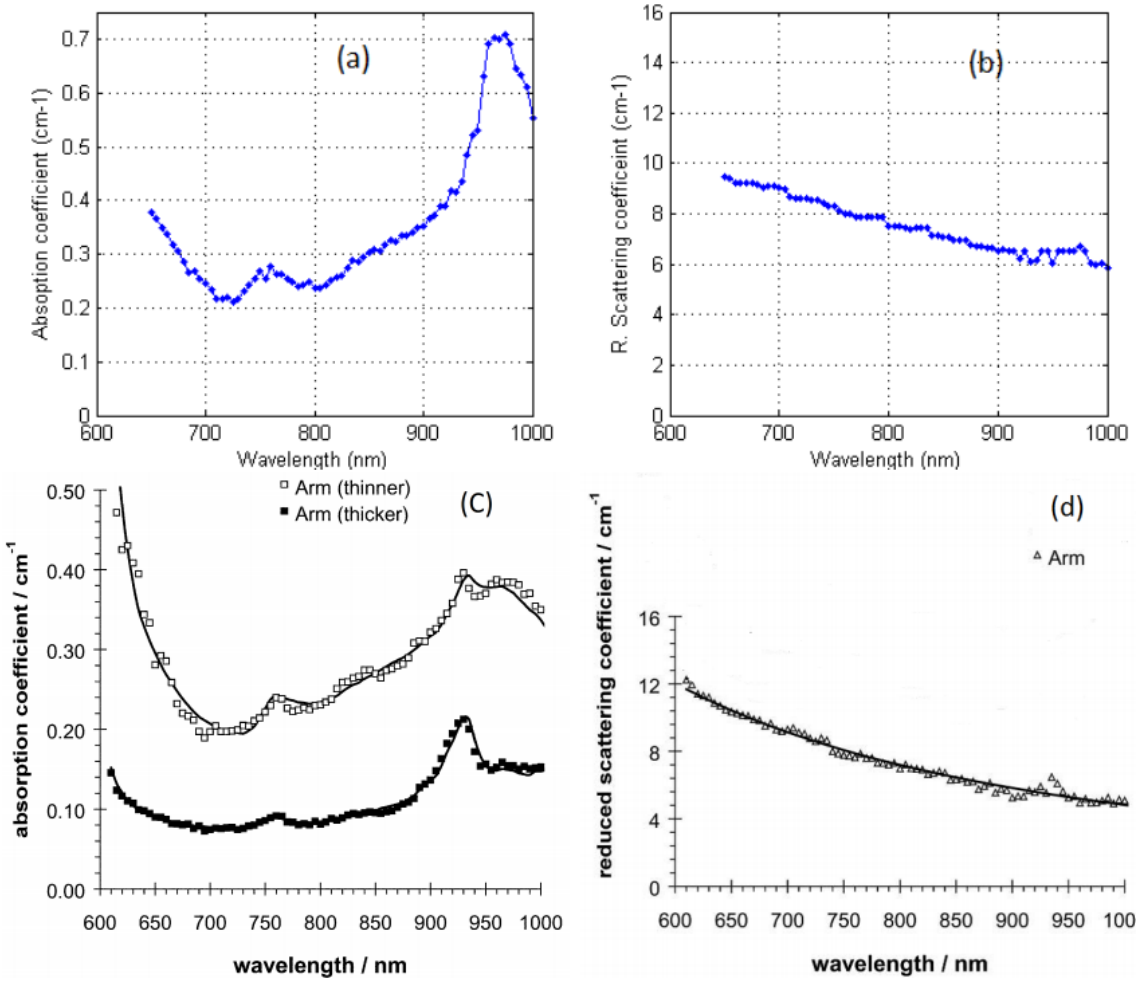

Figure 17: Absorption and scattering spectra taken with 20 mm fibre separation. The data represented by (a) and (b) comes from [7] and the data represented by (c) and (d) comes from [19].

Comparing the absorption and scattering spectra in figure 17 to figure 10 one can see clear similarities in the shape of the curves, and the scattering spectra show good correspondence. The data for male 1, 2 and 3 follow the shape of "Arm(thinner)" from [19] and the data from [7], while the the data for female 1

follow the shape of "Arm(thicker)" from [19]. The measured data share a common haemoglobin peak around $760\ \mathrm{nm}$, but with different amplitudes. The curves for male 1, 2 and 3 have here a similar amplitude to the curve from [7], and the curve for female 1 have similar amplitude to the curve for "Arm(thicker)" from [19]. The absorption peak around $920\ \mathrm{nm}$, which is due to lipids in the subdermis is the most prominent peak for female 1 and is consistent with the data for "Arm(thicker)" from [19], but this peak is not very prominent for male 1, 2, and 3. For male 1, 2 and 3, the water absorption peak at $970\ \mathrm{nm}$ is more prominent and the data is consistent with that from [7] and for "Arm(thinner)" from [19].

The above mentioned similarities between the measurements made in this thesis and the measurement data given by the other two independent sources ([7] and [19]), give a greater factor of relevancy for the measurements made in this thesis.

The high water peak at $970\ \mathrm{nm}$ seen for the curve represented by (a) in figure 17 is higher than the absorption peak for water at this wavelength ($\mu_a \approx 0.5$ for 100% water). This matter is discussed in [7] where the WMC evaluation method is affected by the sample geometry change made by the fibres when put in contact to the subject's skin. The same system (used by [7]) was used to obtain the spectra in figure 10, but here the water absorption peaks are lower and closer to $\mu_a = 0.5$. Male 1 and 2 do have an absorption peak higher than $0.5\ \mathrm{cm}^{-1}$, which could be explained by what is discussed in ref. [7] (see below).

Looking at the STD plotted for male 1 emphasis the conclusion of the study in ref. [7], which gives insight into how the data can change between measurement occasions when the fibres are pressed against the skin with different strengths. Compressed tissue gives the probability of fewer photons escaping over the boundary, which means that more photons with a shorter time of flight will reach the detector and alter the ratio between late and early photons, yielding a higher μ_a value when using the WMC model.

5.1.2 The PMT detector system

The measured data for the longer wavelengths (950 - $1340\ \mathrm{nm}$) shown in figures 13-16 are compared to the data given in figure 18. The scattering follow the reference curve pattern quite well, as well does the absorption showing the prominent lipid/water peak at around $1200\ \mathrm{nm}$. The amplitude of the curves have a similarity below $1000\ \mathrm{nm}$, but this similarity fails to hold for longer wavelengths, which might be explained by the increasing absorption probability, correlated with the difference in collection time between the measurements made in this bachelor work and the measurements presented in [7] ($3\ \mathrm{s}$ compared to $5\ \mathrm{s}$ used in [7]).

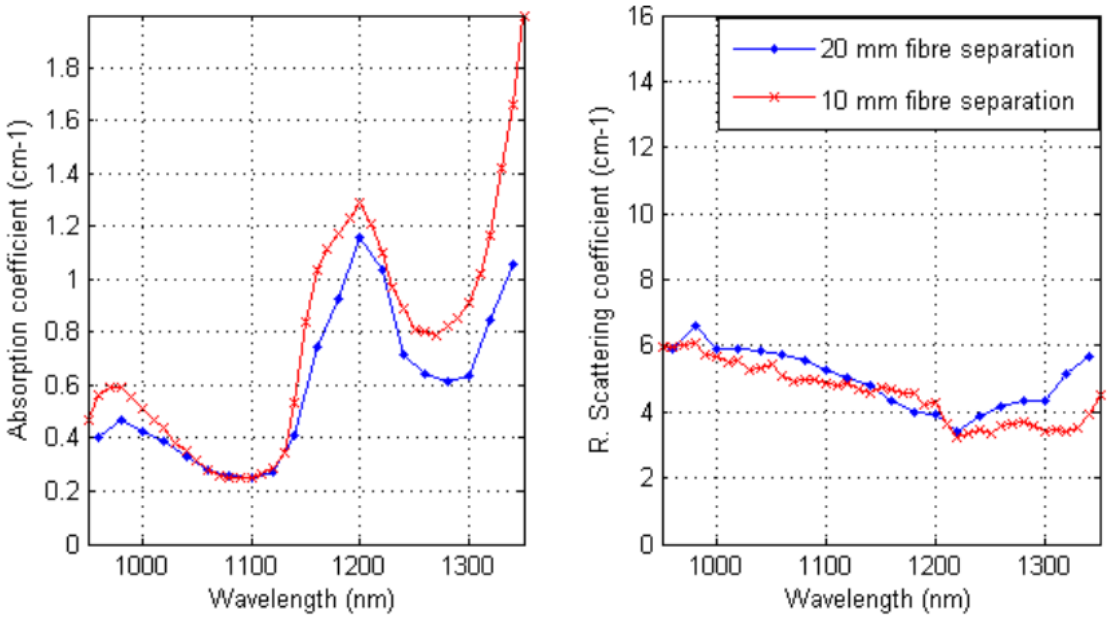

Figure 18: Absorption and scattering spectra taken with 20 *and* 10 mm *fibre separation [7].*

5.2 Comparison of the measured spectra

The primary question for this thesis was to find out if there is any possibility for a trend of the tissue optical properties between different individuals. To assess this one need to go back to the figures presented in section 4 where the results for the measurements made in this thesis are given. When it comes to absorption in the NIR1 range, the data representing female 1 is much lower in amplitude than the data representing male 1, 2 an 3. The major explanation to this is that the photons from the measurements made on female 1 did not reach the muscle tissue, due to the thickness of the subcutaneous fat. This also explains the prominent lipid peak for female 1 at 920 nm, which is not as prominent for the male subjects. One way to increase the depth the photons travel, to actually measure muscle tissue for female 1 is to increase the fibre separation, according to a general rule of thumb that say that this depth is $\propto 1/3$ of the fibre separation. This was not made, which consequently makes it difficult to asses any trend for muscle tissue absorption using the data for female 1, leaving the data for the male subjects to be discussed.

The NIR1 absorption spectra in figure 10 for male 1 and 3 are similar in amplitude regarding the haemoglobin absorption peak at 760 nm, while having a different amplitude regarding the water absorption peak at 970 nm. The water peak at 970 nm for male 3 lies within the statistical variation of the data for male 1, which implies that the peak for male 3 could be lower in amplitude if another measurement with lower fibre pressure would be made, since this seems to induce the largest error in absorption. The spectrum for male 2 is consistently lower than the curves for both male 1 and 3, but share a similar shape. A possible explanation to this is that male 2 has less oxygenated haemoglobin in his muscles, or that male 2 has a higher concentration of lipids (note a small peak at about 920 nm)

enabling a smaller amount of photons to see the muscle tissue.

Another possible explanation to the difference between the measured data for the male test subjects, could be the concentration of the chromophore melanin, but this seems not to be the case. The spectral fit (see figure 12) made to the data in figure 10 follows the shape of the curves quite well for shorter wavelengths, but not for longer wavelengths (above $900\ \mathrm{nm}$), where water and lipid have higher absorption probability. This implies that the melanin concentration values shown in table 1 can be used in a comparison between the different test subjects. Here one can see a similar concentration value of melanin for the test subjects, except for Female 1, which might be an effect of the actual fitting procedure, since the photons propagates through less water, $\mathrm{hb0}_2$, hb, and through more lipids, in this particular case. There is, excluding female 1, a potential to assume that the difference in melanin (includes pigment) between the different test subjects is of no major importance when analysing the measurements. Note that there lies uncertainties in the later part of the curves in figure 12, which mostly arises from the fit to the water and lipid absorption values. Here a possible error might be arising from the reference data on the μ_a for water and lipid.

When it comes to comparing the extracted lipid concentration from the fit in figure 12 between the different test subjects, there is a notable difference in lipid concentration between female 1 and male 1, 2 and 3. There is even a negative value for the lipid concentration for male 3, which implies inaccuracies in the fit made. A possible explanation for this error in the fit considering lipid concentration for male 1, 2 and 3 is that the absorption by lipids is masked by the absorption by water, which is notably seen around $920\ \mathrm{nm}$ where lipid has an absorption peak. If this explanation for the error in the fit is assumed, the model used that created the fit is not applicable for investigation of lipid concentration when the concentration of water is greater (or much greater) than the lipid concentration. In this bachelor work the fit could not be used for investigating lipid concentration for male 1, 2, 3, which is possibly due to the uncertainty of the fibre pressure related to the measurements.

The comparison of the spectra in the NIR2 range is more difficult because of the high absorption attained here, which resulted in lower count rates. It was difficult to evaluate the data using the WMC model and the data above $1340\ \mathrm{nm}$ for male 2 and and 3 had to be discarded. The collection time could have been increased from $3\ \mathrm{s}$ to above $5\ \mathrm{s}$ but this would force the test subjects to be measured upon for a too long time (it already takes more than 45 minutes for a measurement).

Since the fibre distance is the same using the PMT system for the NIR2 measurements, the data for female 1 again shows dominant absorption from lipids and is for this reason not comparable to the male subjects' data for the $15\ \mathrm{mm}$ fibre distance. The data for the male subjects have a promising relation, where the more muscular subject (male 3) has higher levels of collagen, elastin and water absorption. Yet, the difference between the curves for the male subjects is not

very evident until the high absorption for water and lipids around $1200\ \mathrm{nm}$ kicks in. Here the measurements were difficult to evaluate and e.g the fluctuations between measurements on male 1 are of the order of cm^{-1}, which could also be an effect of different fibre pressure (male 3 seem to have been under this effect as well).

When it comes to scattering in the NIR1 range, the curves of the different subjects tend to decrease in a similar way. The amplitude of the scattering seems to vary the most for female 1 compared to male 1 (see figures 8 and 9), which could be a consequence of the higher lipid concentration for female 1, and thus imply that the structure of muscle tissue is more symmetric. Since the scattering varies as it does between the measurements, it is difficult to asses the results in figure 11. The same conclusion goes for the scattering in the NIR2 range, where the shape of the curves here as well are very similar.

There are many measurement factors that contribute to inaccuracies/uncertainties in the measurements made for this thesis. The mentioned factor of fibre pressure to the skin of the subjects plays a major role (more visible for absorption for the measurements), but where on the lower arm the measurements are made is also a major factor, especially for scattering. The last mentioned factor might be a factor creating difficulty in the comparison for scattering, since scattering depend on the amount of particles and structure, and the lower arms of the subjects have different lipid to muscle ratio depending on position. How still a subject were, the pressure on the arm from the fibre holder brick, and the pressure on the arm from the equipment that held it in a fixed position are also factors that contribute to inaccuracy. The last two mentioned factors might give an impact on the blood flow and thus water circulation in the arm, which would effect the absorption.

Despite all practical factors that need to be counted for coupled to performing the actual measurements, the obtained data do have a clear potential for a trend of the optical properties of human muscle tissue in the lower arm when it comes to absorption. The term trend in this thesis emphasizes the possibility to assume a human muscle tissue absorption and scattering template (taking concentration or thickness of fat in consideration), which can be used to detect anomalies in muscle tissue.

6 Conclusions & Outlook

Time-Of-Flight Spectroscopy is a measurement technique that has a potential future for clinical use. Although there is a need for improvements regarding the measurement procedure, the potential is there, as is the potential for a usable template (a trend).

A greater amount of measurements on the different subjects and measurements on a larger magnitude of subjects would be needed to strengthen the possibility for the desired trend. More measurements would also give more valuable information about the scattering, which was insufficient in this bachelor work. The amount of time for this work was limited, which made it difficult to perform more measurements.

The fibre pressure to the skin is one of the main factors that yielded inaccuracies for the evaluated absorption. It would be interesting to see if there is a minimum for the pressure to the skin, in which the geometry alteration is too small to significantly increase the evaluated absorption.

Another thing that could be implemented in further research is a model connecting body fat and optimal fibre distance to actually measure muscle tissue, which would aid in the investigation of muscle tissue for individuals of all body types.

7 Acknowledgements

I would like to thank my supervisors Patrik Lundin and Professor Stefan Andersson-Engels, who have guided me throughout this bachelor work. This thesis would not have been possible to do without your help. Thank you for your positivity and commitment, it really helped. I would also thank Patrik Lundin for explaining the TOFS system and how it worked, and for his ability to always be there when I really needed his help on matters I could not comprehend myself.

One person that especially aided me a lot during this bachelor work is Emily Emilsson. I would not have been able to complete this thesis without your tremendous support and your help in the lab.

I would also like to thank my friends Said Ali, Sukant Chaudhary and Ola Brange for their support and contribution to the measurements. Sadly the software crashed both times Sukant was measured upon.

8 References

[1] J.W. Spliethoff, D.J. Evers, H.M. Klomp, J.W. Sandick, M.W. Wouters, R. Nachabe, G.W. Lucassen, B.H.W. Hendriks, J. Wesseling, T.J.M. Ruers. Improved identification of peripheral lung tumors by using diffuse reflectance and fluorescence spectroscopy. *Lung cancer*, 80(2):165-171, 2013.

[2] A.M.K. Nilsson, R. Berg, S. Andersson-Engels. Measurements of the optical properties of tissue in conjunction with photodynamic therapy. *Applied optics*, 34(21):4609-4619, 1995.

[3] P. Lundin, E.K. Svanberg, L. Cocola, M. lewander Xu, G. Somesfalean, S. Andersson-Engels, J. Jahr, V. Fellman, K. Svanberg, S. Svanberg. *Noninvasive Monitoring of Gas in the Lungs and Intestines of Newborn Infants using Diode Lasers: Feasibility Study*. J. Biomed. Opt. 18(12):127005, 2013.

[4] T. Svensson. *Pharmaceutical and Biomedical Applications of Spectroscopy in the Photon Migration Regime*. Ph.D. thesis, Lund university, 2008.

[5] Ashley J. Welch, Martin J. C. van Gemert (Eds.). *Optical-Thermal Response of Laser-Irradiated Tissue 2nd ed.*. Springer Netherlands, 2011.

[6] Ishimaru. *Wave Propagation and Scattering in Random Media*. Academic, New York VOL. 1, Chap. 7, p. 147, 1978.

[7] S. Strömblad. *Measuring the Optical Properties of Human Muscle Tissue using Time-of-Flight Spectroscopy in the Near Infrared*. Master's Thesis, Lund University, LRAP-498, 2015.

[8] E. Emilsson. *Time of Flight Spectroscopy in Human Muscle Tissue*. Bachelor thesis, Lund University, 2015.

[9] E. Alerstam. *Optical Spectroscopy of Turbid media: Time-Domain Measurements and Accelerated Monte Carlo Modelling*. Ph.D. thesis, Lund University, 2011.

[10] A. Shaharin. *Photon Time-of-Flight and Continuous-Wave Near-Infrared-Spectroscopy of Human Skeletal Muscle Tissue; A Comparative Study*. Master's thesis, Lund university.

[11] A.A Subash. *Wide-Bandwidth Time of Flight Spectroscopy of Turbid Media*. Master's thesis, Lund university.

[12] Hochschule Koblenz. *Introduction to Tissue Optics*
URL https://www.hs-koblenz.de/rac/fachbereiche/mut/forschung-projekte/labore-projekte/labor-fuer-biomedizinische-optik/forschung/introduction-to-tissue-optics/

[13] T.J Allen, A. Hall, A. P. Dhillon, J.S Owen, P.C. Beard. *Spectroscopic Photo Acoustic Imaging of Lipid-Rich Plagues in the Human Aorta in the 740 to 1400 nm Wavelength Range*. J. Biomed. opt. 17(6), 2012.

[14] A.N. Bashkatov, E.A. Genina and V.V Tuchin. *Optical Properties of Skin, Subcutaneous, and Muscle Tissues: A Review*. Journal of Innovative Optical Health Sciences Vol. 4, No. 1, 9-38, 2011.

[15] Fianium LTD
URL http://www.fianium.com

[16] Micro Photon Devices
URL http://www.micro-photon-devices.com

[17] W. Becker. *The bh TCSPC Handbook, 6th edition*. Becker & Hickl GmbH
URL http://www.becker-hickl.com/index.html

[18] Oregon Medical Laser Center. *Optical Properties Spectra*.
URL http://omlc.org/spectra/, 2015-05-12.

[19] P. Taroni, A. Pifferi, A Torricelli, D. Comelli, and R. Cubeddu. *In Vivo Absorption and Scattering Spectroscopy of Biological Tissues*. Photochem. Photobiol. Sci. 2, 124-129, 2003.